PHYSICAL REVIEW C VOLUME 3, NUMBER 5 MAY 1971

Excitation of the Giant Resonance in ^{12}C by Inelastic Electron Scattering

A. Yamaguchi, T. Terasawa, K. Nakahara, and Y. Torizuka
Laboratory of Nuclear Science, Tohoku University, Sendai, Japan
(Received 8 October 1970)

The longitudinal and transverse form factors were determined separately as functions of the excitation energy from 15 to 40 MeV in the momentum-transfer range 0.75–1.56 F^{-1}. For some of the form-factor spectra the measurements were extended up to an excitation energy of 100 MeV and the results were compared with the quasielastic model presented by de Forest. The q dependence of the experimental form factors for levels were compared with the predictions of the particle-hole model and with the intermediate-coupling model. We have then found the levels with the following excitation energies (MeV), spins, and parities: 18.1 (1^-), 18.6 (3^-), 19.6 (4^-), 20.0 (2^+), 20.6 (3^+), 21.6 (3^-), 22.0 (1^-), 22.7 (1^-), and 23.8 (1^-). We have also found new evidence of the possibility of the spin-isospin mode for the 22.7-MeV (1^-) excitation.

I. INTRODUCTION

Inelastic electron scattering from nuclei using deeply penetrating high-energy electrons is very useful as a means of elucidating the nuclear structure[1, 2]; in particular, for an investigation of the giant-resonance region.[3-17] The giant resonance has been studied from photodisintegration,[18, 19] photon total absorption,[20] and inverse reactions such as the (p, γ) reaction.[21, 22] In the case of these reactions the momentum transfer q is determined uniquely by the excitation energy. On the other hand, in electron scattering the momentum transfer can be varied for a fixed energy transfer. This is the advantage of electron scattering over photonuclear studies. However, some difficulties in the analysis of the electron scattering data have remained. In an inelastically scattered electron spectrum, two types of continuum backgrounds under the giant resonance have been considered; one is the "radiation tail" due to electrons degraded by the radiative effects, and the other may be due to electrons scattered quasielastically from the individual nucleons in the nucleus. The former can be subtracted successfully by a calculation, since the basic interaction of the electron with the target is well known. However, an estimate of the latter appears to be complicated, particularly in the giant-resonance region.

Recently, the quasielastic model of nuclear electroexcitation has been generalized by de Forest.[23] As a main feature of this theory, the effects of nuclear binding and the distortion of the wave function of the final-state nucleon are included in an energy-dependent nuclear potential. Then, quasielastic scattering can be treated in the framework of the independent-particle model. According to de Forest's suggestion, quasielastic scattering is not distinct from the single-particle excitation of bound states or resonances; thus, the concept of a quasielastic background in the giant-resonance region is unrealistic.

We have carried out high-resolution measurements of inelastic electron scattering from the ^{12}C giant resonance at various incident electron energies and scattered angles. For some of the cross-section spectra at an incident energy of 250 MeV, the measurement was extended up to an excitation energy of 100 MeV. After subtracting the radiative tail by a computer code, the spectra were compared with the predicted cross sections of the quasielastic model. Satisfactory agreement is obtained between theory and experiment.

The de Forest model predicts a smooth curve corresponding to the sum of the strengths for the single-particle excitations of all the multipole states. This theory is thus incapable of describing the complicated structure which is seen in the giant-resonance region. For such fine structure, detailed descriptions have been provided by the particle-hole models with the Tamm-Dancoff or random-phase approximation, as will be mentioned later.

The electron interacts with the nucleus not only through the transverse interaction corresponding to the photon case, but also has the possibility of a longitudinal interaction. By carrying out the measurements at different angles (relatively, forward and backward) keeping the momentum transfer constant, one can extract the longitudinal and transverse form factors squared as functions of the excitation energy $[|W_L(q, \omega)|^2$ and $|W_T(q, \omega)|^2]$. Such a procedure is particularly useful in the giant-resonance region as a means of isolating a complicated structure, since the form factors of some levels are either almost completely longitudinal or transverse. Then, we could find many levels which were marginally apparent from previous studies. The usual form factors $[|F(q)|^2]$

for these excitations are immediately obtained from the generalized form factor. To identify the spin and parity of the level, its form factor as a function of the momentum transfer is compared with the theoretical form factor (squared) calculated by making use of the one-particle–one-hole model presented by Vinh Mau and Brown,[24] Gillet and Vinh Mau,[25] Lewis and Walecka,[26] de Forest[27] (later referred to as LWD), and Donnelly.[28] Although this j-j coupling approximation does not provide accurately the magnitude of the experimental form factor, it has been recognized that its q dependence is well reproduced with this theory by assuming a multipole operator which may be associated with the level observed. For the levels considered to have even parity, the experimental form factors are compared with the predictions of the intermediate-coupling model presented by Boyarkina.[29] In some cases, such as for the giant dipole resonance, its form factor is compared with Kamimura, Ikeda, and Arima (later referred to as KIA) model[30] which introduced a coupling of the quadrupole vibration with the dipole oscillation in the framework of the particle-hole approximation. The KIA form factors were calculated using the wave functions of force I in the present comparison.

The generalized Goldhaber-Teller model[9, 31, 32] regards nuclear matter as made up of four interacting fluids which build the oscillations of the four modes, such as the isospin (τ) mode, the spin-isospin (σ-τ) mode, etc. However, it is possible to understand the extended fluid model in terms of the nuclear shell model; the τ states are $L=1$, $S=0$, and thus $J=1^-$; and the σ-τ states are $L=1$, $S=1$, and thus $J=0^-$, 1^-, 2^-. Lewis and Walecka[26] have pointed out that the two electric-dipole states predicted at 23 and 25 MeV make up the giant dipole resonance in ^{12}C. The level at 23 MeV has a dominant $(1d_{5/2}, 1p_{3/2}{}^{-1})$ configuration which corresponds to the τ-mode oscillation which can be strongly excited by the longitudinal interaction. However, the component $(L=1, S=1)$ of the σ-τ mode is also contained in this 23-MeV state and can be seen from the q dependence of its transverse form factor. The other level at 25 MeV with a dominant $(1d_{3/2}, 1p_{3/2}{}^{-1})$ configuration corresponds almost to a pure σ-τ mode and is dominantly excited by the transverse interaction. The relative magnitude of the transverse form factors for these 23- and 25-MeV states changes with increasing momentum transfer, and the majority of the contribution shifts from the former to the latter.[26, 33] Though such transitions are actually observed near the predicted energies, the magnitudes of their form factors do not change in the same manner as theory predicts.[13, 26, 33, 34] One of the present experimental purposes is to examine the presence of the σ-τ states. We have found new evidence of this mode for 22.7-MeV (1^-) excitation observed.

Our longitudinal and transverse form factors in the selected energy region were compared with the theoretical form factors predicted by the quasielastic and particle-hole models mentioned above. The magnitudes of the experimental form factors are well reproduced by the theoretical curves of the quasielastic model. Our transverse form factors are also compared with those obtained from previous electron scattering at 180° using low-energy electrons[3, 9, 11] along with the curve predicted by above theory. Our longitudinal and transverse form factors are further compared with recent data in a q range 0.36–0.84 F^{-1} obtained at the National Bureau of Standards.[35]

II. EXPERIMENTAL METHOD

The primary beams of the accelerator were deflected by an achromatic beam transport system consisting of a quadrupole magnet between two bending magnets. Three slit systems were used; two of them were placed with 5.5-m intervals between the accelerator and first bending magnet to fix the location and direction of the beams; the other was the energy-defining slit installed at the middle of the two bending magnets. The beams were refocused on the target by a quadrupole doublet magnetic lens placed 7.2 m upstream from the target. Two pairs of steering coils were provided to adjust horizontal and vertical deflections, respectively. The size and location of the beam spot at the target was monitored by a closed-circuit television using a BeO screen with appropriate markings. This screen was frequently inserted in the beam during the experiment by remote control. After passing through the target, the beams were monitored by a secondary-emission monitor (SEM) using a conventional current integrator. The efficiency of the SEM was calibrated against a Faraday cup. The electrons scattered from the target were analyzed by a magic-angle $(\theta=169.7°)$[36, 37] double-focusing magnetic spectrometer of 100-cm central radius of curvature. The field was monitored by a commercial rotating-coil fluxmeter. The spectrometer magnet was mounted on a turntable which could rotate about a central post on which a target chamber was mounted. The angle of rotation for the spectrometer extended from 35 to 145° in usual use. A target ladder accurately placed at the center of the target chamber held five targets including a BeO screen and a thick graphite target for the calibration of the counter efficiency. The targets could be moved or vi-

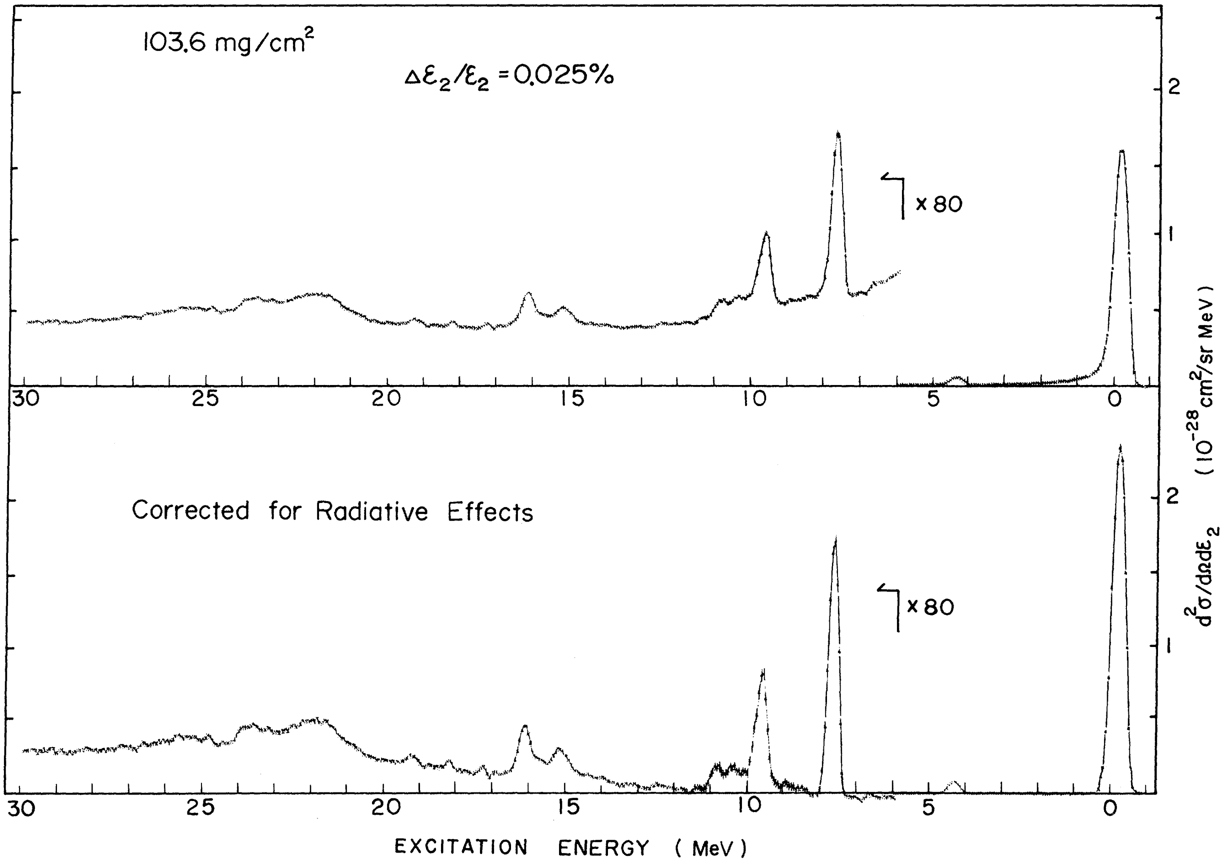

FIG. 1. Spectrum of electrons scattered from ^{12}C at a scattering angle of 35° and incident energy of 250 MeV. The data points were taken at intervals of $\Delta\epsilon_2/\epsilon_2 = 0.025\%$. The abscissa gives values of the excitations energy up to 30 MeV. The ordinate gives the cross section in the unit of 10^{-28} cm^2/sr MeV. The upper plot shows data points corrected for dead-time losses and for counter efficiencies. The lower plot shows the same data with the radiative effects corrected.

brated by remote control.

The scattered electrons exited the target chamber through a Mylar window, passed through a vacuum foil (aluminum) at the entrance of the spectrometer, were deflected by the magnetic field, and were detected by a 33-channel detector ladder, which covers a 3.3% range in momentum. Each channel consisted of three Li-drifted silicon detectors working as a counter telescope. Because of the low background rate of the solid-state detector, unlike the case of a plastic scintillator, the (slow) coincidences among three elements were handled in a computer system during pulse-to-pulse intervals. Data collection, display on an oscilloscope during measurement, and correction of counting efficiency were also provided by a computer.

The spectrum of the scattered electrons was taken by shifting the setting of the magnetic field in steps of $\Delta\epsilon_2/\epsilon_2 = 3.3\%$, ϵ_2 being the energy of the scattered electron. For each setting of the magnetic field, the location of the counter system was moved by remote control 1.81 mm stepwise along the focal plane, corresponding to a momentum shift of 0.025%. Finally, the data points were collected at intervals of $\Delta\epsilon_2/\epsilon_2 = 0.025$ or 0.05%.

The relative efficiency of each channel was measured using an inelastic continuum region of ^{12}C, however, it may be incorrect to regard this continuum as completely flat. To smear out some structures which may be present, the measurement was carried out by increasing and decreasing the magnetic field corresponding to the continuum. The slope of the continuum was measured by counting the same peak or structure with a different portion of the multichannel detector.

An example of the scattered electron spectrum for ^{12}C is shown in the upper part of Fig. 1. Except for the radiative correction, all data points were corrected for the spectrometer dispersion, counter dead-time losses, and counter efficiency. Many peaks may be seen superimposed on the radiation-tail background due mainly to the elastic peak.

The radiative effects which are due to the radiation of electrons as they traverse the target remove electrons from a given point of the spectrum and spread them out in a spectrum of lower energy. The former effect reduces the peak area and the latter forms a background under the inelastic peaks which is called a radiation tail. The corrections for these effects were performed with an iterative-procedure code[38] using a computer.

As a first step the spectrum is divided into a number of successive bins of interval ΔE. Then, the highest-energy interval or first bin is multiplied by a factor $e^{\delta}[\lambda/(\lambda-1)]$ that corrects for electrons removed from the energy interval of that bin.

$$\left(\frac{d\sigma}{d\Omega}\right)_{\text{real}}=\left(\frac{d\sigma}{d\Omega}\right)_{\Delta}e^{\delta_s(\Delta E)+\delta_b(\Delta E)}\left(\frac{\lambda}{\lambda-1}\right), \qquad (1)$$

where $(d\sigma/d\Omega)_{\Delta}$ is the cross section corresponding to the area of interval of ΔE; and $\delta_s(\Delta E)$, $\delta_b(\Delta E)$, and $\lambda/(\lambda-1)$ are the terms due to Schwinger radiation,[39-41] thick-target bremsstrahlung,[42] and collision losses,[43] respectively.

Next, the subtraction of the radiation tail is made. The number of radiation-degraded elec-

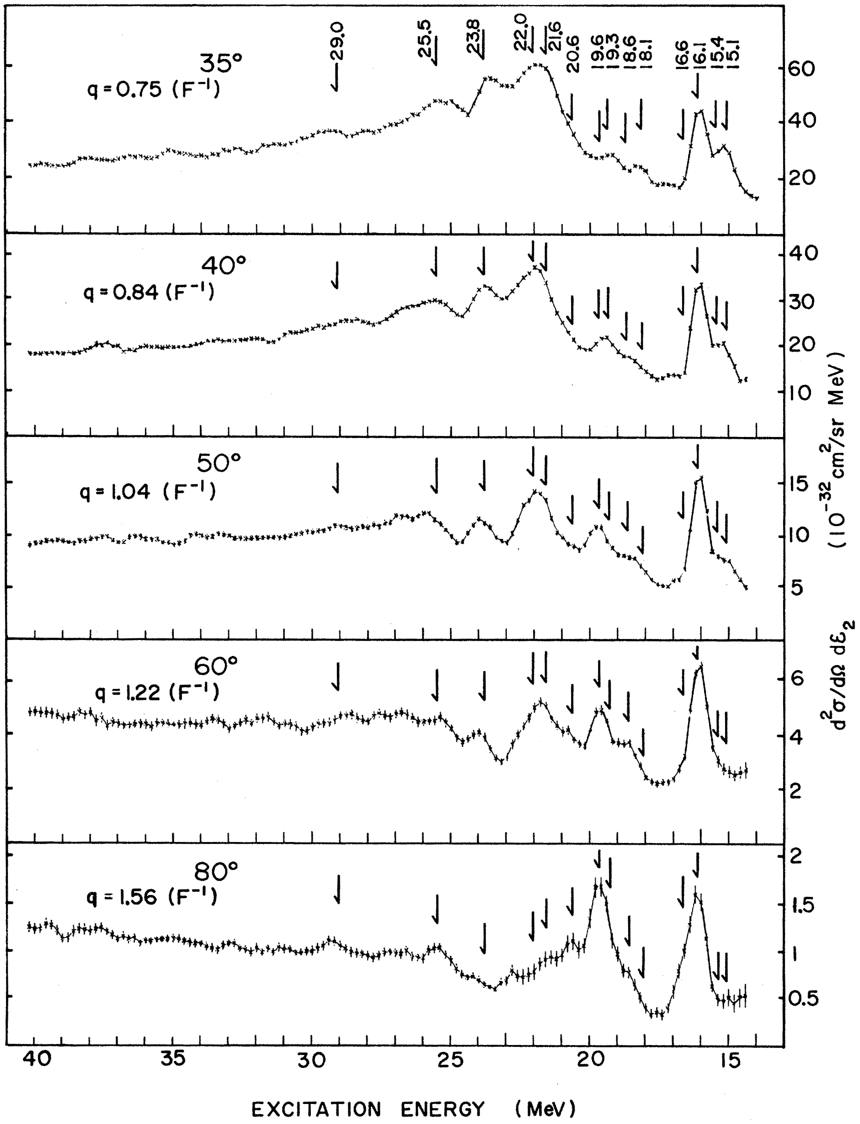

FIG. 2. Spectra of scattered electrons at 35, 40, 50, 60, and 80° from ^{12}C for the incident energy of 250 MeV. The cross section is shown in the unit of 10^{-32} cm^2/sr MeV. The arrows indicate the positions of the peaks. The values of momentum transfer for each spectrum were calculated assuming an excitation energy of 25 MeV.

trons in each subsequent bin that come from the first-bin electrons that would be there without radiation was computed with the Isabelle-Bishop formula[44] and subtracted from each subsequent bin. Then, the same procedure is applied again to the second bin and continued until all the bins have been corrected.

The spectrum with these corrections applied is shown in the lower part of Fig. 1. Usually the bin interval ΔE was made equal to the interval of data points. The accuracy of the code used can be seen by comparing the calculated tail with the measured one below an energy (7 MeV) of the particle-emission threshold. In the most serious case ($\epsilon_1 = 250$ MeV, $\theta = 35°$), the radiation tail in the giant-resonance region amounts to about 26% of the measured counting rate. This type of background decreases rapidly as the incident electron energy or scattering angle is increased.

The thickness of the graphite target was chosen to be 104, 187, or 500 mg/cm^2 depending on the experimental condition. The over-all resolution was determined by the beam-spread, target-thickness, and spectrometer-resolution effects. To measure all of the spectra with almost the same resolution, the beam spread was varied from 0.13 to 0.2%, depending on the energies of the incident electrons, by adjusting the energy-defining slit.

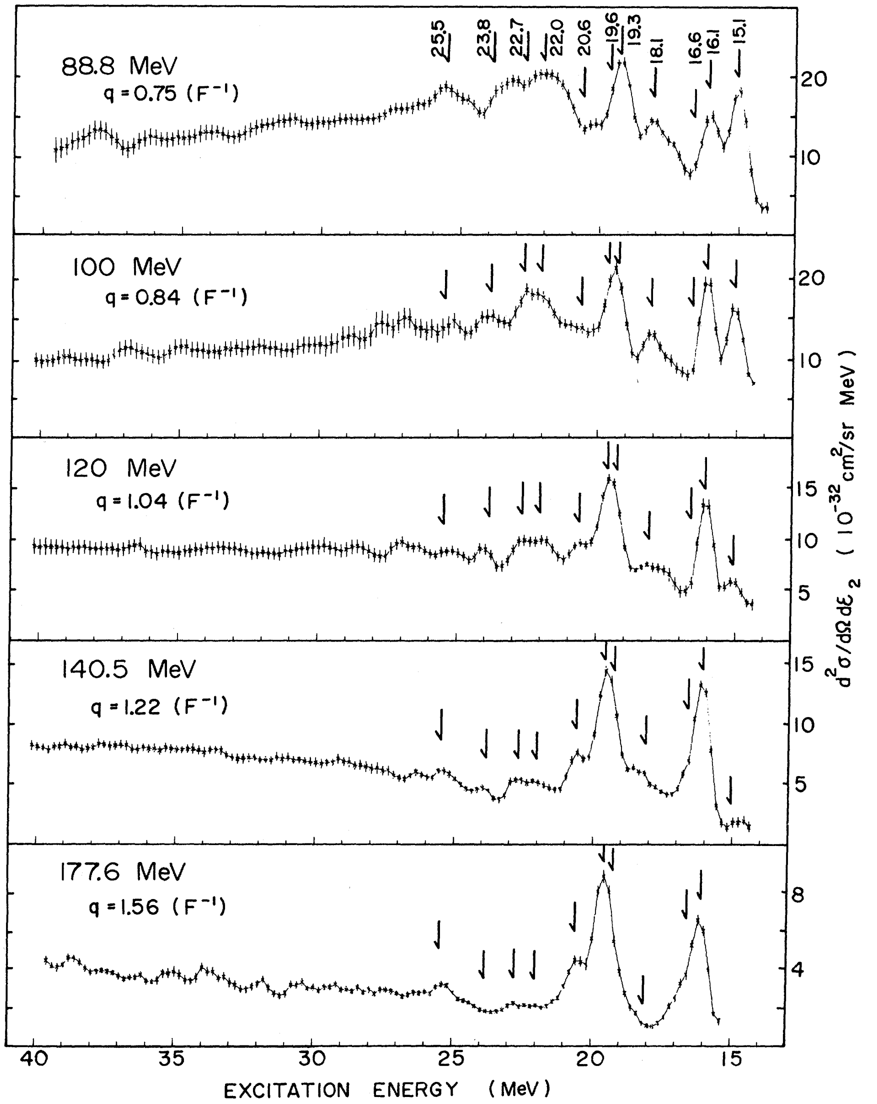

FIG. 3. Spectra of scattered electrons at 135° from ^{12}C for the incident energies of 88.8, 100, 120, 140.5, and 177.6 MeV. These energies were chosen to give the same momentum transfer as the values of the corresponding forward-angle spectra in Fig. 2.

The absolute cross section of inelastic electron scattering was obtained by comparing its yield with the elastic-peak area. The cross section of elastic scattering from ^{12}C is well known from previous studies.[45]

III. ANALYSIS AND RESULTS

In Figs. 2 and 3 we present inelastically scattered electron spectra in ^{12}C up to an excitation energy of 40 MeV measured at the various angles with the various incident electron energies. Such spectra show a complicated structure in the energy region of the giant resonance. According to the particle-hole calculation, high-lying levels are excited by either almost the pure longitudinal or transverse interaction, or by both. Thus, it seems to be of great importance to determine separately the longitudinal and transverse form factors. Such a procedure is performed with the help of the first-order Born approximation.

In the Born approximation for the interaction of the electron with the nucleus, the cross section for electron scattering is given by

$$\frac{d^2\sigma}{d\Omega d\epsilon_2}=\sigma_{\text{Mott}}\,|F(q)|^2\delta(E_2+\epsilon_2-E_1-\epsilon_1), \qquad (2)$$

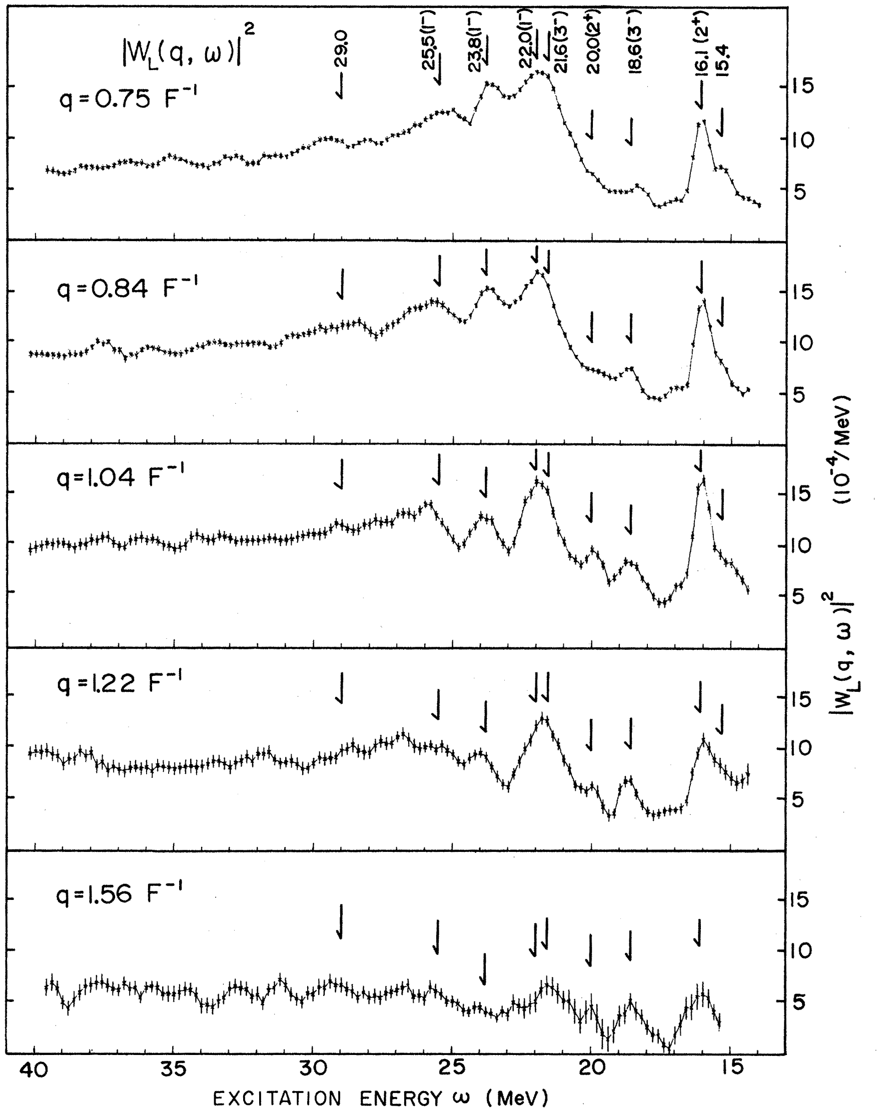

FIG. 4. The longitudinal form factors $|W_L(q,\omega)|^2$ for electroexcitation in ^{12}C over the excitation energy range from 15 to 40 MeV corresponding to momentum transfers of 0.75, 0.84, 1.04, 1.22, and 1.56 F^{-1}. The arrows show the positions of the form-factor peaks. The spins and parities assigned from the present and previous studies are shown in the parentheses.

$$\sigma_{\text{Mott}}=\frac{Z^2e^4\cos^2\frac{1}{2}\theta}{4\epsilon_1{}^2\sin^4\frac{1}{2}\theta}, \tag{3}$$

where $F(q)$ is the total form factor defined by this relation, σ_{Mott} is the Mott cross section for elastic electron scattering through an angle θ of an electron of energy ϵ_1 from a point, spinless nucleus of charge Ze with no recoil, and $\epsilon_{1,2}$ and $E_{1,2}$ are the total energies of electron and nucleus, respectively; the subscripts 1 and 2 refer to the initial and final states.

The form factor $W(q, \omega)$ for the small excitation-energy intervals of ϵ_2 and $\epsilon_2+\Delta\epsilon_2$ is defined as

$$|W(q, \omega)|^2=\frac{1}{\Delta\epsilon_2}\int_{\Delta\epsilon_2}|F(q)|^2\delta(E_2+\epsilon_2-E_1-\epsilon_1)d\epsilon_2\,. \tag{4}$$

Here ϵ_2 is related to the excitation energy ω by

$$\epsilon_2=\frac{\epsilon_1-\omega}{1+(2\epsilon_1\sin^2\frac{1}{2}\theta)/M_T}, \tag{5}$$

where M_T is mass of the target nucleus. Using Eq. (5), $W(q, \omega)$ is written in the form

$$|W(q, \omega)|^2=\frac{1}{\Delta\omega}|F(q)|^2\,.$$

$W(q, \omega)$ is further expressed by the Born approximation as

$$|W(q, \omega)|^2=\frac{q_\mu{}^4}{q^4}|W_L(q, \omega)|^2+\left(\frac{q_\mu{}^2}{2q^2}+\tan^2\tfrac{1}{2}\theta\right)|W_T(q, \omega)|^2, \tag{6}$$

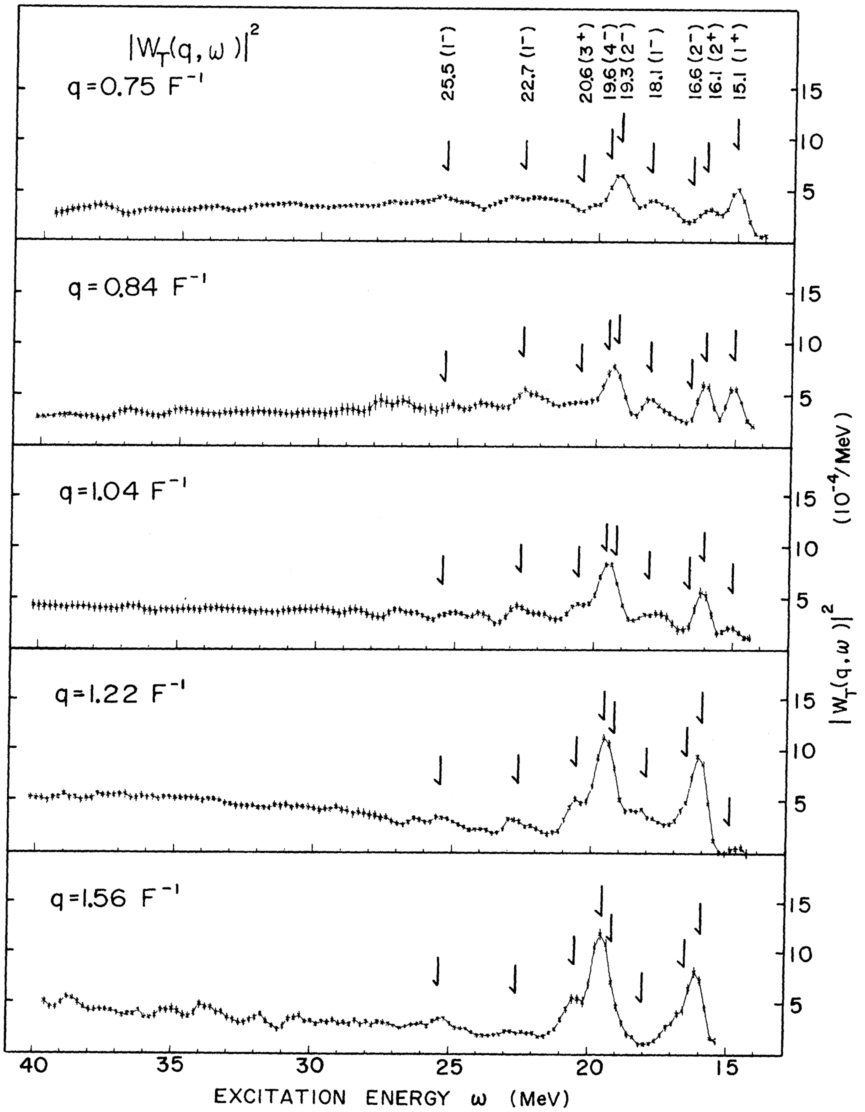

FIG. 5. The same as for Fig. 4 except that the transverse form-factors $|W_T(q,\omega)|^2$ are shown.

where $W_L(q, \omega)$ is the part of the total form factor due to the Coulomb or the longitudinal interaction and $W_T(q, \omega)$ is the part due to the transverse interaction. The four-momentum of the electron is $k_\mu = (\vec{k}, i\epsilon)$. The momentum transfer is $q_\mu = (\vec{q}, i\Delta\epsilon) = k_{1\mu} - k_{2\mu}$. The usual form factor is related to the form factor $W(q, \omega)$ by

$$|F(q)|^2 = \int_\omega |W(q, \omega)|^2 d\omega . \qquad (7)$$

In order to determine the longitudinal and transverse form factors using Eq. (6), the cross sections are taken at different angles (relatively forward and backward), keeping the momentum transfer constant. The forward-angle cross sections corresponding to q values of 0.75, 0.84, 1.04, 1.22, and 1.56 F^{-1} were taken at angles of 35, 40, 50, 60, and 80° with an incident electron of 250 MeV, and the backward-angle data were taken at 135° by adjusting the incident electron energy to give the same momentum transfer as above. In our kinematical calculation, q was obtained by assuming an excitation energy of 25 MeV. The values of q were corrected for the change of wavelength of the incident electron when it passes through the nucleus. This correction factor is $\gamma = (1 + 3Z\alpha/2k_1R)$,[46]

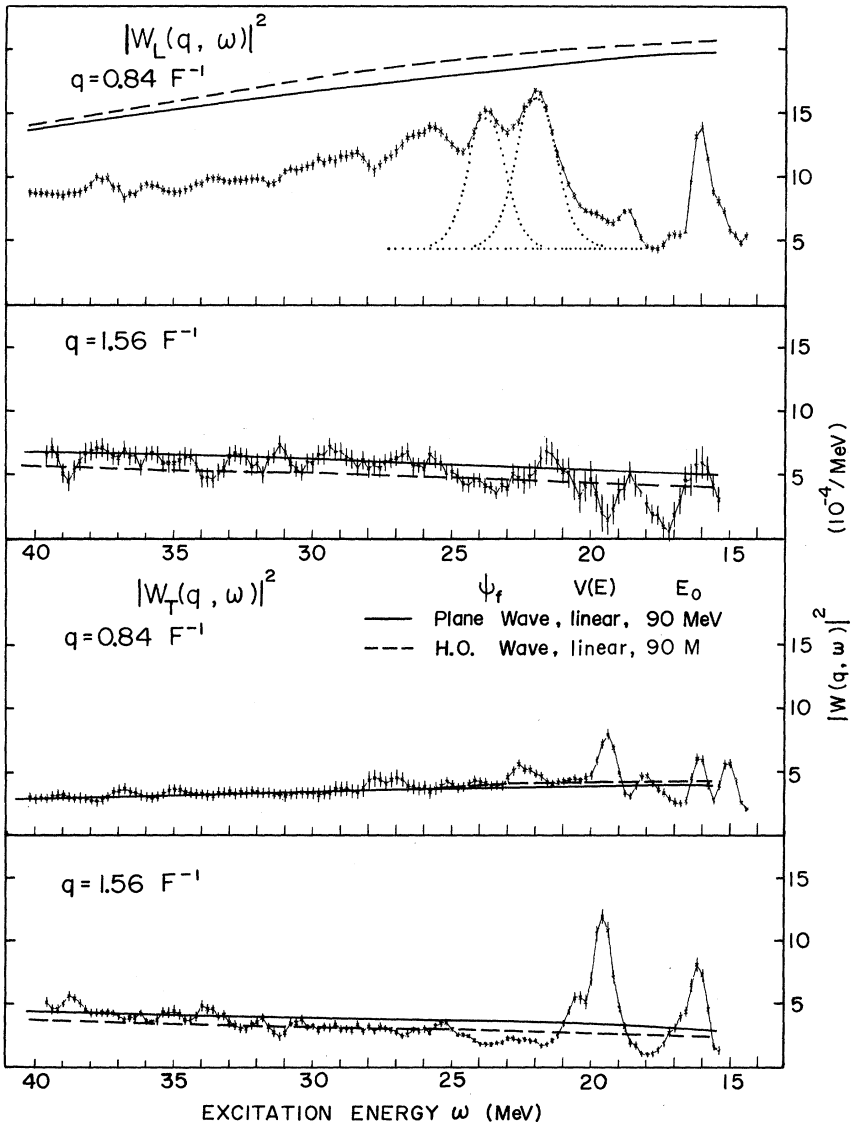

FIG. 6. The longitudinal and transverse form-factor spectra are compared with the theoretical longitudinal and transverse form factors calculated using the quasielastic model. Both calculations with the plane and harmonic-oscillator wave functions show almost the same result. Also shown are the resonance shapes and continuum background for the 22.0- and 23.8-MeV peaks (dashed).

where α is the fine-structure constant and R is the equivalent uniform-nuclear-charge radius. Then, incident electron energies in the backward-angle experiments were selected so that $q'(250\ \mathrm{MeV}, \theta) = q'(\epsilon_1, 135°)$, where $q' = \gamma q$.

All the inelastic spectra obtained as functions of the excitation energy from 15 to 40 MeV were divided into the successive bins of the same interval of 200 keV, and then the cross-section points were averaged within the bin intervals. The results of this procedure are shown in Figs. 2 and 3. Then, the longitudinal and transverse form factors for each bin, whose excitation energy is assumed at the bin center, were calculated using Eq. (6) and plotted as shown in Figs. 4 and 5. The width of the resolution function of these spectra (650 keV) is greatly increased over that of the primary spectra (~400 keV) by above procedure. However, the peaks are more clearly isolated than those of the primary spectra, since the form factors for excitation of some states are either almost completely longitudinal or transverse. In the longitudinal form factor of Fig. 4, dominant peaks may be seen at 16.1, 18.6, 20.0, 21.6, 22.0, 23.8, 25.5, and possibly 29 MeV superimposed on a smooth continuum. In the transverse form factor, there are peaks at 15.1, 16.1, 18.1, 19.3, 19.6, 20.6, 22.7, and 25.5 MeV. The area of the form-factor peaks for the levels other than the giant dipole resonance was determined by a fitting procedure using the shape of the elastic peak (650 keV). The quasielastic background (knock-out-nucleon process) may contribute to the continuum at energies ≥20 MeV. However, we have not yet employed any theoretical calculation for the estimation of the quasielastic background. For the distinct peaks seen in the giant-resonance region, the continuum (background) was estimated so as to give the same resonance shape among the peaks corresponding to the same excitation energy but different momentum transfers. One example is shown in the upper part of Fig. 6 (dashed curve). The shape is almost Gaussian with a width of 1.5 MeV. The form factors for the 15.1-, 16.1-, 16.6-, 18.1-, 18.6-, 19.3-, 19.6-, 20.0-, 20.6-, 22.7-, 22.0-, and 23.8-MeV states are plotted as functions of q as shown in Figs. 7–16 where the data from previous studies are also included.

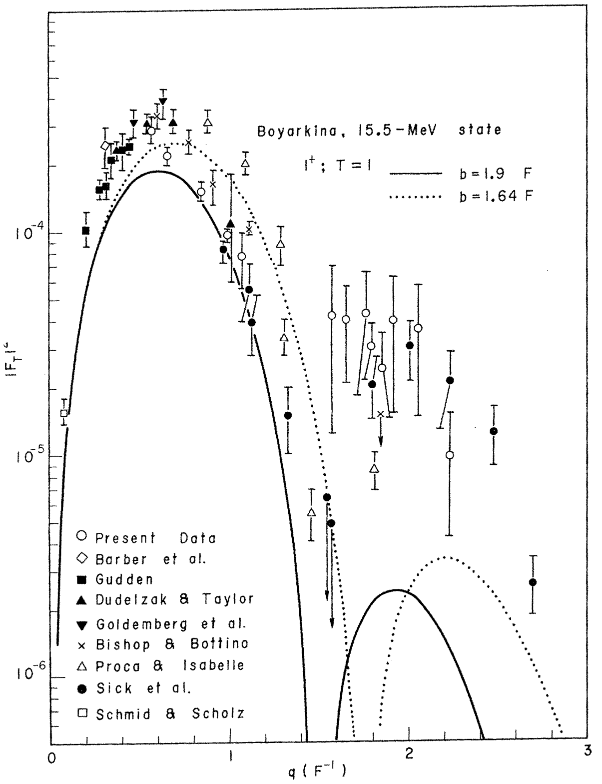

FIG. 7. The transverse form factor for the 15.1-MeV level. Previous data (Refs. 3–7, 14, 15) are also plotted. The curves were calculated using the intermediate-coupling model (Boyarkina) with the different oscillater-length parameters b.

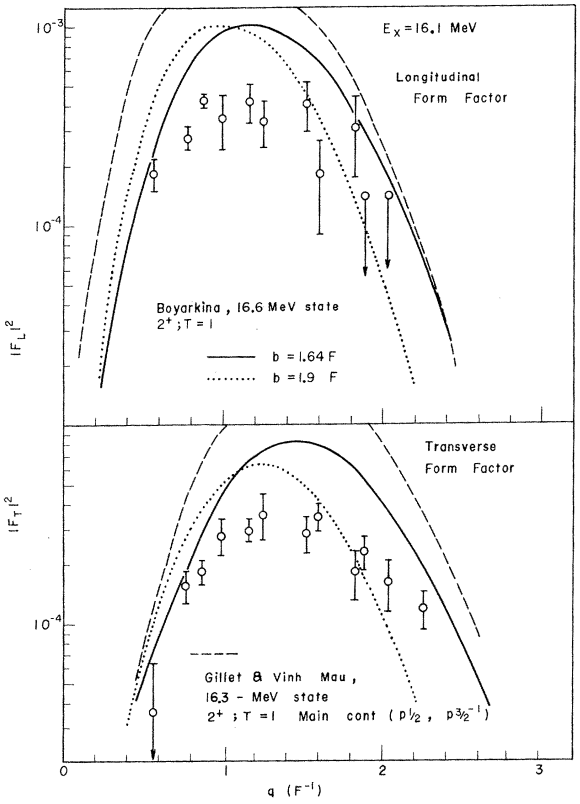

FIG. 8. The longitudinal and transverse form factors for the 16.1-MeV level. The curves correspond to the particle-hole model (Gillet and Vinh Mau) with $b = 1.64$ F (dashed), the intermediate-coupling model (Boyarkina) with $b = 1.64$ F (solid), and with $b = 1.9$ F (dotted).

Furthermore, the longitudinal and transverse form factors in the selected energy regions such as 21–26, 26–37, and 21–37 MeV are shown as functions of q in Figs. 17–20. The previous electron-scattering data corresponding to these energy regions are also summarized in the same figures.

IV. COMPARISON WITH NUCLEAR MODELS

A. Quasielastic Model

The cross sections for electroexcitation in ^{12}C displayed up to an excitation energy of 100 MeV are compared with the theoretical curves of the quasielastic model presented by de Forest.[23] This theory treats all of the one-particle excitations in the framework of the independent-particle model. The effects of binding and the distortion of the wave function of the final-state nucleon are included in an energy-dependent nuclear potential. The form of this potential was chosen to have a linear dependence of $V(E) = \text{const} \times (E - E_0)$ on E or an exponential dependence of $V(E) = \text{const} \times e^{-E/E_0}$. As optimum values of E_0 de Forest found about 90 MeV for the linear form $V(E)$ and 100 MeV for the exponential form. In the present comparison, we have used both forms, treating E_0 as an adjustable parameter. Both the plane wave function and the harmonic-oscillator wave function were used as the wave function of the final-state nucleon. Antisymmetrization effects were not considered, although they seemed to be important in the giant-resonance region.

The predictions of this model are compared with our spectra at the scattering angles of 40 and 80° with an incident electron energy of 250 MeV. As shown in Fig. 21, both models [the plane wave function and harmonic-oscillator (H.O.) wave function] are able to predict the main feature of the cross section quite well. Some discrepancies which may be seen in the small-ω region may result from ignoring the antisymmetrization effects. According to de Forest's example, the magnitude of the cross section around an excitation energy of 25 MeV declines about 20% with the inclusion of antisymmetrization. The plane-wave calculation (solid curve), though it seems to give a better approximation in the large-ω region, somewhat underestimates the absolute magnitude of the cross section near $\omega = 90$ MeV as seen in the upper spectrum, while it overestimates in the case of the lower spectrum. When E_0 is varied markedly to 50 MeV, the agreement in this region is achieved, as can be seen; however, the over-all agreement

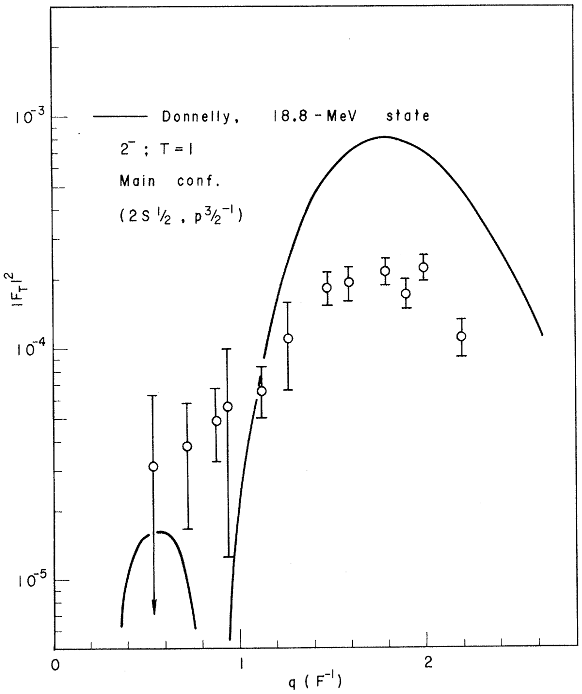

FIG. 9. The transverse form factor for the 16.6-MeV level. The theoretical transverse form factor for the magnetic quadrupole state with a dominant $(2s_{1/2},\ p_{3/2}{}^{-1})$ configuration (Donnelly) is also shown.

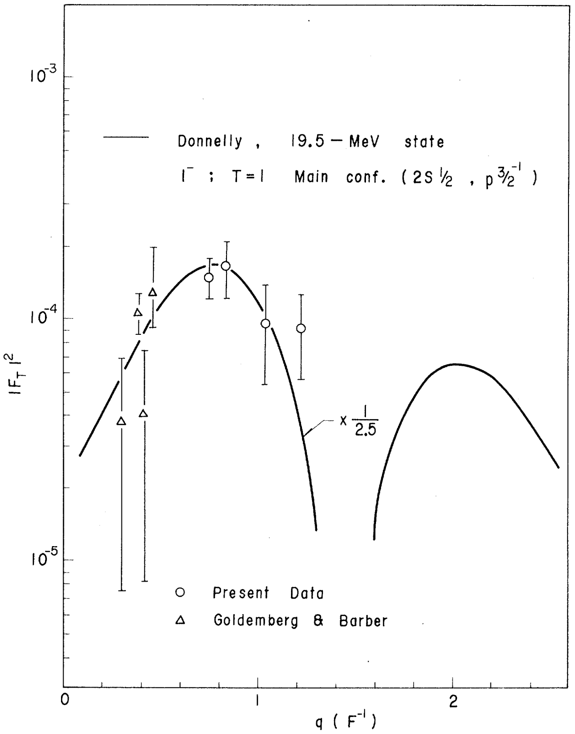

FIG. 10. The present transverse form factor and the previous data Ref. 11 for 18.1-MeV state are plotted. Also shown is the theoretical transverse form factor for the electric dipole state with a dominant $(2s_{1/2},\ p_{3/2}{}^{-1})$ configuration (Donnelly).

is not improved.

A more detailed comparison may be made by using the form-factor spectra separated into the longitudinal and transverse components. The longitudinal and transverse form factors up to an excitation energy of 40 MeV at $q=0.84$ and 1.56 F^{-1} are compared with the theoretical form factors of the de Forest model as shown in Fig. 6. A gross agreement between theory and experiment is quite satisfactory. Some discrepancy for the longitudinal form factor at 0.84 F^{-1} may be removed by considering the antisymmetrization effects as mentioned above.

For the next comparison, the longitudinal and transverse form factors in the selected energy regions of 21–26 and 26–37 MeV were plotted as functions of q in Figs. 17 and 18. The transverse form factor measured at 180° by previous electron scattering experiments and the longitudinal and transverse form factors obtained at NBS are also shown in the same figure. The general agreement between the theoretical and experimental form factors is seen to be good. The harmonic-oscillator wave function gives, however, a better representation, particularly in the low-q range. Although the quasielastic model cannot describe the fine structure, the success in predicting the absolute magnitude of the experimental cross section or form factor is remarkable. The present experimental result agrees with the previous one within the experimental errors.

B. Particle-Hole Model and Intermediate-Coupling Model

In the longitudinal form factors shown in Fig. 4, dominant peaks may be seen at 16.1, 18.6, 20.0, 21.6, 22.0, 23.8, and 25.5 MeV superimposed on a smooth continuum. In the transverse ones, there are peaks at 15.1, 16.1, 16.6, 18.1, 19.3, 19.6, 20.6, 22.7, and possibly 25.5 MeV as seen in Fig. 5.

The present study is characterized in the measurement in the high-momentum-transfer range where high-multipole states can be excited dominantly. We have found many peaks for which spins and parities have not been established from previous studies. It seems to be useful to compare our form factors with the theoretical ones calculated by using the wave functions of a nuclear model such as the particle-hole model or the interme-

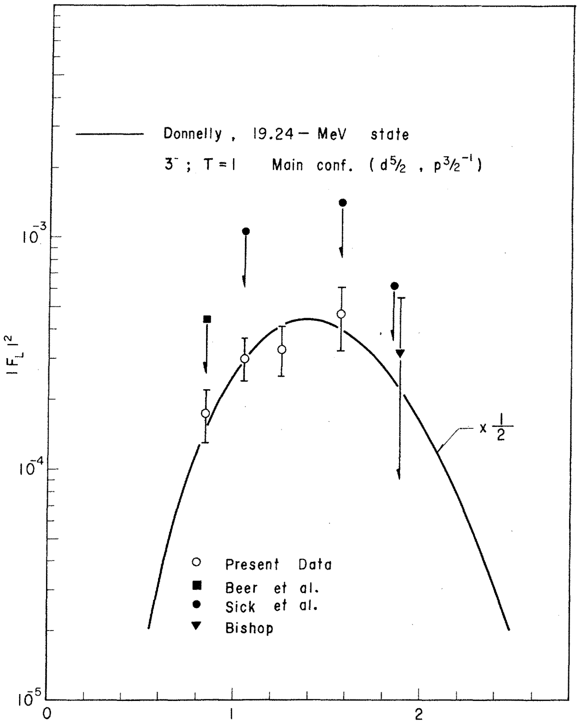

FIG. 11. The present longitudinal form factor for the 18.6-MeV state and the previous data (Refs. 8, 10, 15) are plotted. Shown is the theoretical longitudinal form factor for the octupole state with a dominant ($1d_{5/2}$, $1p_{3/2}{}^{-1}$) configuration.

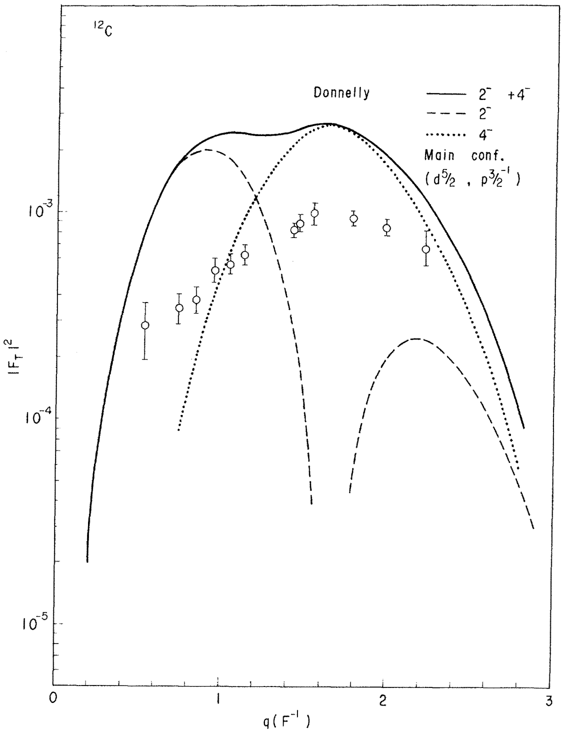

FIG. 12. The transverse form factor for the 19-MeV complex. The dashed and dotted curves correspond to the 20.6-MeV (2^-, $T=1$) and 20.17-MeV (4^-, $T=1$) states with a dominant ($1d_{5/2}$, $1p_{3/2}{}^{-1}$) configuration (Donnelly), respectively. The solid curve is the sum of both contributions.

diate-coupling model. Although such a microscopic model does not account for the absolute magnitude of the form factor accurately, its q dependence is well characterized by the matrix element with the multipole operator properly chosen. The particle-hole model has been calculated by Lewis and Walecka,[26] de Forest,[27] and Donnelly[28] in a reformulation or an extension of the Brown-Gillet model[24,25] by assuming a j-j coupling spherical nucleus for the ground state. Among these calculations Donnelly has presented all of the possible multipole states in ^{12}C as listed in Table I. We will compare our form factors mainly with his result. For even-parity states, the experimental form factor will be compared with the theoretical form factor calculated by making use of the intermediated-coupling model presented by Boyarkina.[29]

The 15.1-MeV (1^+, $T=1$) state has been extensively examined with experimental and theoretical interest by many authors. Our data for this level were taken in the high-q range corresponding to the second diffraction maximum as shown in Fig. 7 where all of the previous data are also plotted. According to the particle-hole calculation, this level is almost a pure ($1p_{1/2}$, $1p_{3/2}{}^{-1}$) single-particle state. However, it is well known that the magnitude of the form factor for this configuration is larger by about a factor of 4 than obtained from the experiment. Agreement between experiment and theory is improved by the use of the wave function of the intermediate-coupling model as demonstrated by Kurath[47] and Hirooka.[48] Both have calculated the 15.11-MeV form factor by varying the oscillator-length parameter b to provide the best fit to the data. Kurath has suggested $b \approx 2.0$ F; however, it is considerably higher than the value (1.64 F) obtained from the analysis of elastic electron scattering. On the other hand, Hirooka has shown by using a slightly modified Cohen-Kurath wave function,[49] that $b = 1.64$ F is not only consistent with the 15.11-MeV form factor, but also with the other data such as the muon capture rate in ^{12}C or the ft value of the ^{12}B β decay.[50] They have, however, limited their calculation to within the q range of the first diffraction peak. We have extended the calculation up to the q value of the second peak using the Boyarkina wave function. The magnitude of the first peak is well reproduced by the theoretical form factor; however, it does not account for the relative magnitude for the second peak. Recently, Chemtob and Lumbroso[51] have shown that the effect of the meson-exchange currents gives an increase of the form factors particularly at the second peak in agreement with the

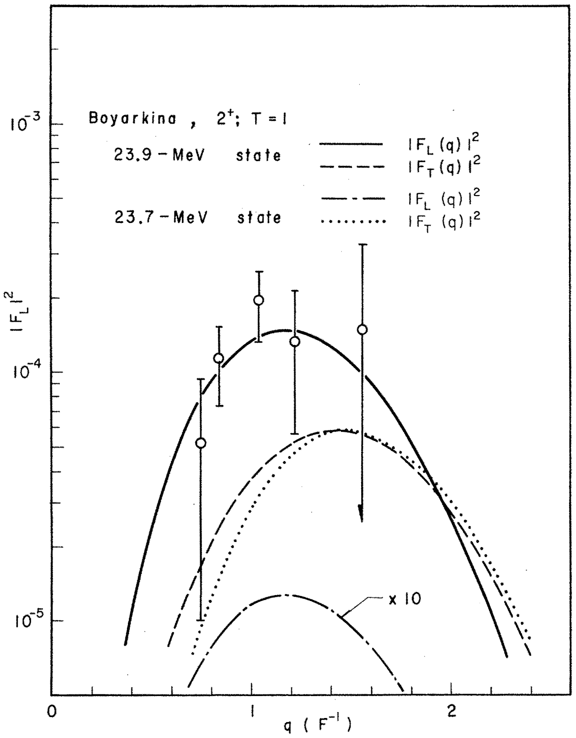

FIG. 13. The longitudinal form factor for the 20.0-MeV level. Also shown are the theoretical longitudinal and transverse form factors for the 23.7- and 23.9-MeV 2^+ $T=1$ states (Boyarkina).

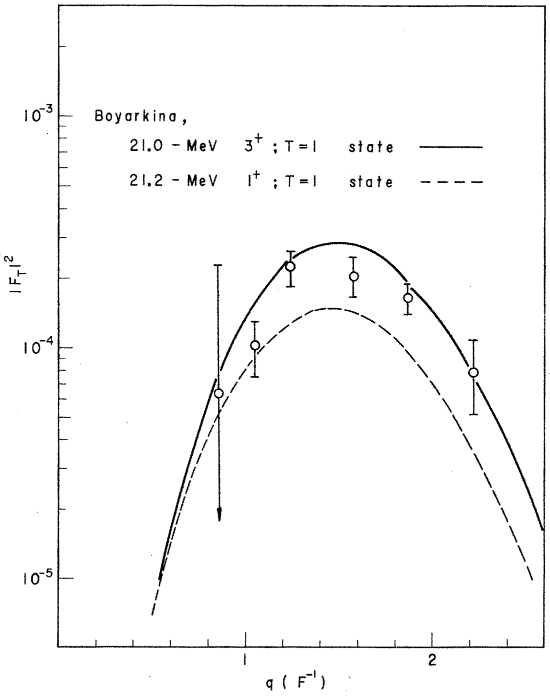

FIG. 14. The transverse form factor for the 20.6-MeV level. The $M1$ and $M3$ form factors calculated using the intermediate-coupling-model wave functions (Boyarkina) are also shown.

experimental observation.

The 16.11-MeV (2^+, $T=1$) level has almost the same configuration as the case of 15.1-MeV level. This level is not only excited by the longitudinal interaction, but also dominantly excited by the transverse interaction through the isovector term in the operator. Both the longitudinal and transverse form factors were separated experimentally as shown in Fig. 8. Also shown are the theoretical form factors calculated with the one-particle–one-hole model (dashed curves) and with the intermediate-coupling model (solid curves). The particle-hole model overestimates the form factor by about a factor of 5 for both the longitudinal and transverse components, whereas the intermediate-coupling calculation well reproduces the experimental data in both cases. In the intermediate-coupling calculation, we used two different oscillator-length parameters of 1.64 and 1.9 F; the former corresponds to the value from the analysis of elastic electron scattering, and the latter provides the best fit to the 15.11-MeV (1^+) form factor[47] as mentioned above. In the 16.11-MeV case the theoretical form factor with $b=1.64$ F gives a better fit to the data than that with $b=1.9$ F as seen in Fig. 8.

Figure 9 shows the experimental form factor for the 16.6-MeV (2^-, $T=1$) level. This excitation is found to be almost completely transverse in accord with the identification as a magnetic quadrupole state. However, the q dependence is quite different from the usual case; the magnitude of the second diffraction peak is markedly larger than the first peak. This feature is well reproduced by the theoretical form factor of the predicted 18.80-MeV (2^-, $T=1$) state with a dominant ($2s_{1/2}$, $1p_{3/2}^{-1}$) configuration (Donnelly).

Figures 4 and 5 show the almost pure transverse excitation at 18.1 MeV which decreases rapidly as q is increased. The 18.1-MeV level was first studied by Barber[11] in the low-q range and was identified as one of the dipole states by Donnelly *et al.*[15] Our transverse form factor for the 18.1-MeV excitation is plotted in Fig. 10 where the data of Goldemberg and Barber[11] are also included. Also shown is the theoretical transverse form factor for the predicted 19.52-MeV (1^-, $T=1$) state (Donnelly).

A 3^-, $T=1$ level at 18.6 MeV was first reported by Feldman, Suffert, and Hanna[52] and further stud-

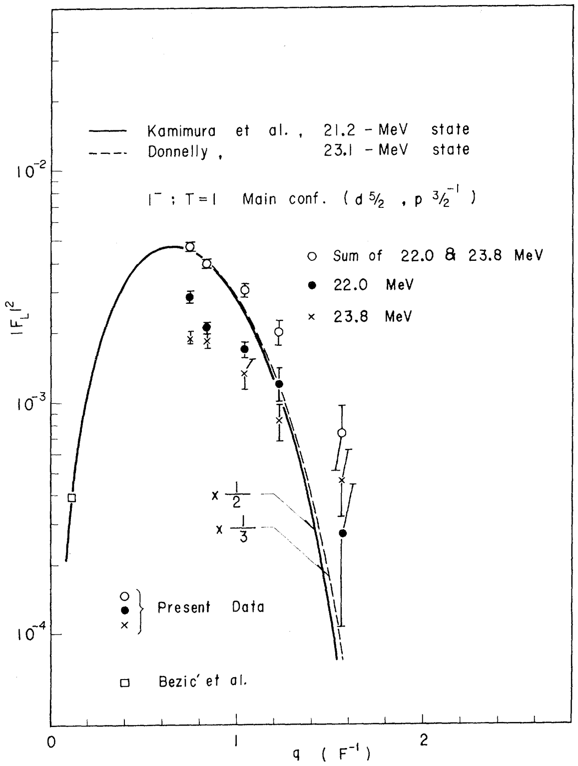

FIG. 15. The longitudinal form factors for the 22.0- and 23.8-MeV levels and the sum of both are plotted against q. The form factors at the photon point were estimated from the data of Bezić *et al.* (Ref. 20). Also shown are the theoretical form factors for the dipole isospin state with a dominant ($1d_{5/2}$, $1p_{3/2}^{-1}$) configuration.

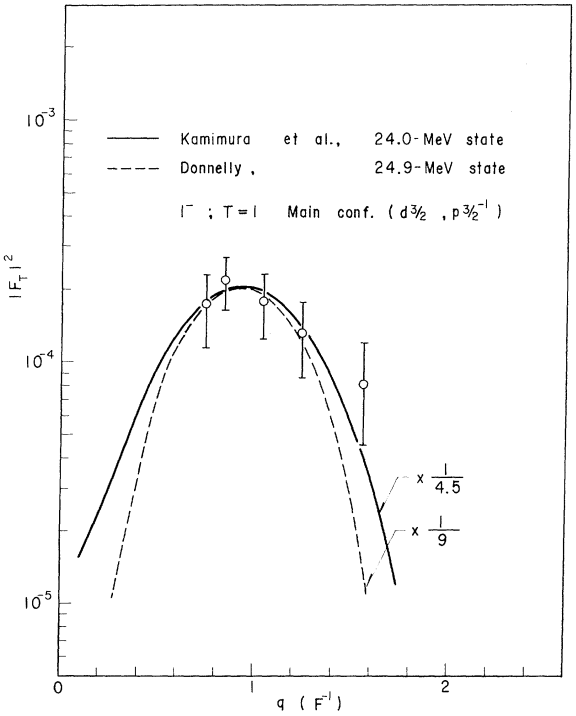

FIG. 16. The transverse form factor as a function of q for the 22.7-MeV peak. The curves correspond to the form factors for the dipole spin-isospin states with a dominant ($1d_{3/2}$, $1p_{3/2}^{-1}$) configuration. The KIA model predicts sizable strength even at the photon point.

ied by Donnelly *et al.*[15] Friar[53] has suggested that the form factor for the excitation of this level is almost pure longitudinal. Our 18.6-MeV form factor is found to be longitudinal in accord with this interpretation. The form-factor points are plotted in Fig. 11 and compared with the theoretical form factor for the predicted 19.24-MeV (3^-, $T=1$) state (Donnelly). The agreement of the previous data which are also plotted in the same figure with ours seems to be reasonable.

As may be seen in Fig. 5, the excitation energy of 19.3 MeV shifts to 19.6 MeV as q is increased. The presence of a 2^- state at 19.3 MeV was confirmed by recent high-resolution low-q experiment.[54] The most prominent peak at 19.6 MeV may correspond to a 4^-, $T=1$ state suggested by Donnelly *et al.*[15] Our transverse form factor for the 19-MeV complex are plotted in Fig. 12. In the same figure the dashed and dotted curves are the theoretical form factors corresponding to the predicted 20.60-MeV (2^-, $T=1$) and 20.17-MeV (4^-, $T=1$) states (Donnelly), respectively.

Figure 13 shows the experimental longitudinal form factor for the 20.0-MeV peak. Boyarkina predicts the second and third 2^+, $T=1$ states at 23.7 and 23.9 MeV. The absolute magnitude of the experimental form factor is well reproduced by the theoretical form factor of the predicted 23.9-MeV state as seen in the same figure.

The peak at 20.6 MeV has been suggested as a 2^-, $T=1$ state with a dominant $(1d_{3/2}, 1p_{3/2}^{-1})$ configuration from the previous study by Torizuka *et al.*[16] The present experiment was extended up to a q value of 2.2 F^{-1} as shown in Fig. 14. Then we have found that the q dependence of the theoretical 2^- form factor is not in accord with the experimental form factor, which seems to be associated with the multipole order 3. The possible 3^-, $T=1$

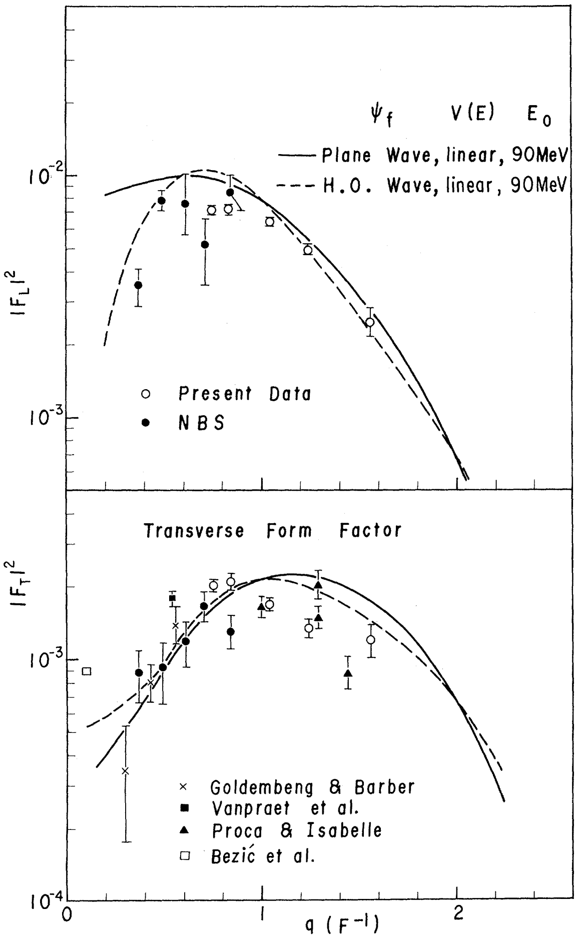

FIG. 17. The longitudinal and transverse form factors as functions of q for a range of 21–26 MeV. The data points of the previous studies (Refs, 3, 9, 11, 20, 35) are also plotted. Also shown are the theoretical results of the quasielastic model with the plane (solid) and harmonic-oscillator (dashed) wave functions.

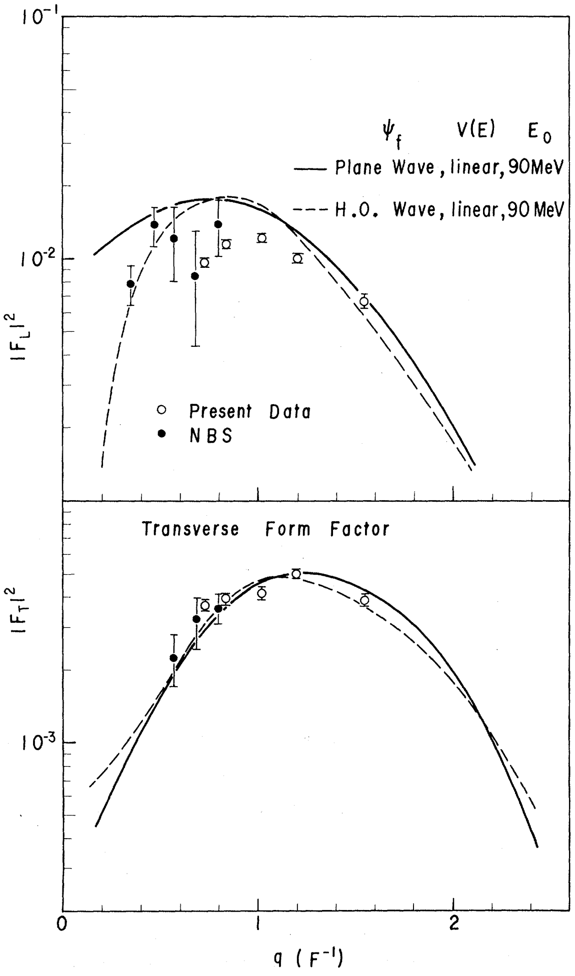

FIG. 18. The same as for Fig. 17 except that the form factors for an extended range of 26–37 MeV are shown.

state predicted at 19.24 MeV with a dominant ($1d_{5/2}$, $1p_{3/2}{}^{-1}$) configuration was identified with the 18.6-MeV peak as mentioned before, and another 25.09-MeV (3^-) state with a dominant ($1d_{3/2}$, $1p_{3/2}{}^{-1}$) configuration has a comparable strength for both the longitudinal and transverse excitations from the particle-hole calculation (Donnelly). As may be seen in Fig. 4, such a longitudinal component is not found near 20.6 MeV. The possibility of 3^+, $T=1$ state for this form factor was then investigated by using the Boyarkina wave function (3^+, $T=1$, $E_x=21.0$ MeV) as shown in Fig. 14. Also shown is the theoretical curve for the 21.2-MeV (1^+, $T=1$) state listed in the Boyarkina table. The q dependence and magnitude of the experimental form factor is well reproduced by both the 1^+ and 3^+ form factors. However, the 3^+ assignment seems to be more probable, since the lowest-lying high-spin

TABLE I. The theoretical and observed energy levels (MeV) for $J^\pi=1^-$, 2^-, 3^-, and 4^-, $T=1$ in ^{12}C.

J^π	Donnelly (Ref. 28)	Main configuration	Present work
1^-	19.52	($2s_{1/2}$, $1p_{3/2}{}^{-1}$)	18.1
	23.09	($1d_{5/2}$, $1p_{3/2}{}^{-1}$)	22.0, 23.8, 25.5
	24.89	($1d_{3/2}$, $1p_{3/2}{}^{-1}$)	22.7, 25.5
	35.55	($1p_{1/2}$, $1s_{1/2}{}^{-1}$)	
2^-	18.80	($2s_{1/2}$, $1p_{3/2}{}^{-1}$)	16.6
	20.60	($1d_{5/2}$, $1p_{3/2}{}^{-1}$)	19.3
	23.83	($1d_{3/2}$, $1p_{3/2}{}^{-1}$)	
3^-	19.24	($1d_{5/2}$, $1p_{3/2}{}^{-1}$)	18.6
	25.09	($1d_{3/2}$, $1p_{3/2}{}^{-1}$)	25.5
4^-	20.17	($1d_{5/2}$, $1p_{3/2}{}^{-1}$)	19.6

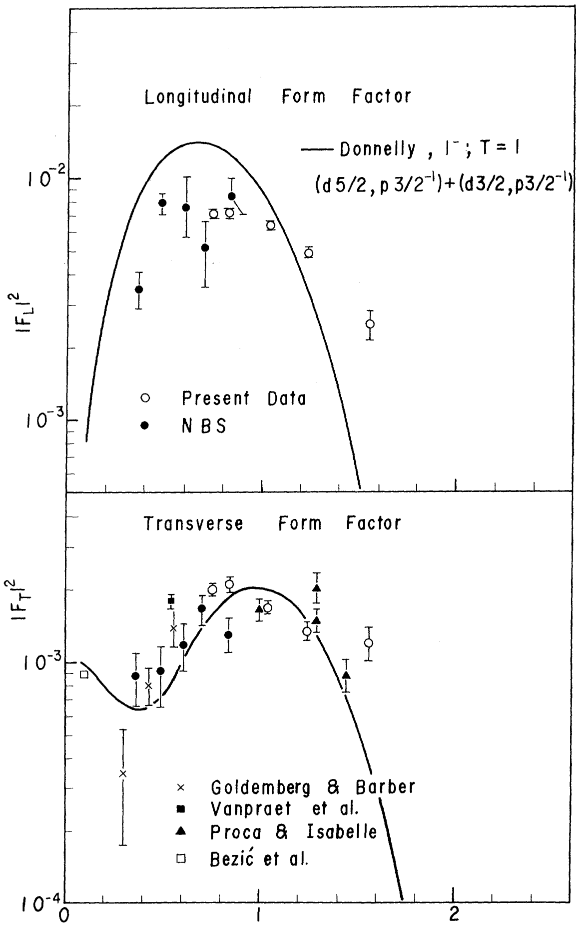

FIG. 19. The data are the same as for Fig. 17. Shown are the theoretical form factors corresponding to the sum of the form factors for the dipole states at 23.09 and 24.89 MeV (Donnelly) with dominant ($1d_{5/2}$, $1p_{3/2}{}^{-1}$) and ($1d_{3/2}$, $1p_{3/2}{}^{-1}$) configurations, respectively.

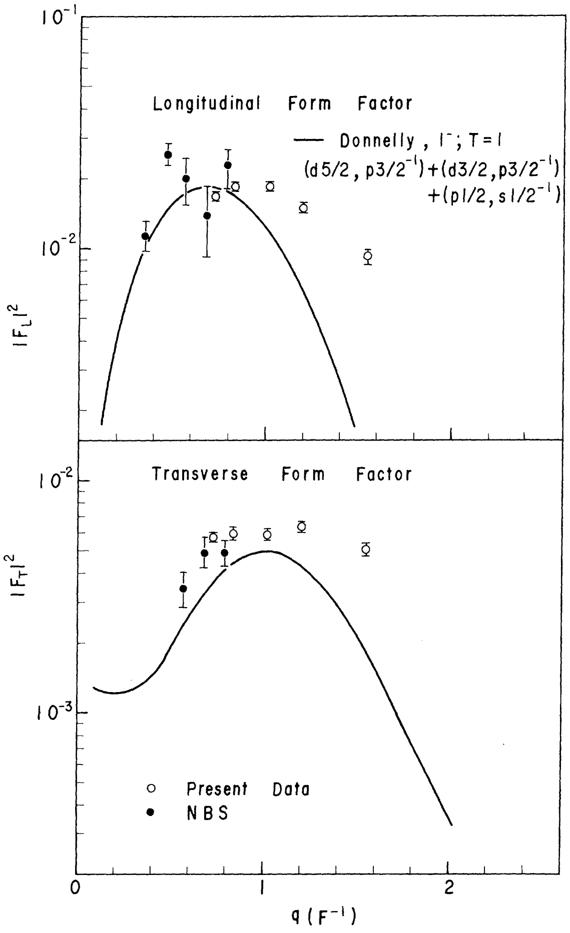

FIG. 20. The longitudinal and transverse form factors for a range of 21–37 MeV are plotted as function of q. The theoretical curves are the sum of the form factors for the dipole states at 23.09, 24.89, and 35.55 MeV (Donnelly) corresponding, respectively, to dominant ($1d_{5/2}$, $1p_{3/2}{}^{-1}$), ($1d_{3/2}$, $1p_{3/2}{}^{-1}$), and ($1p_{1/2}$, $1s_{1/2}{}^{-1}$) configurations.

state is favorably excited in the usual case.

The longitudinal form-factor peak at 22.0 MeV shifts toward lower excitation energy as q is increased, and then another peak is clearly seen at 21.6 MeV which seems to be a 2^+ or 3^- state. Recently, Antony-Spies *et al.*[54] have predicted the 3^- states in ^{12}C at 18.8 MeV ($T=1$), 20.6 MeV ($T=0$), and 24.8 MeV ($T=1$). The first seems to correspond to the 18.6-MeV (3^-) state as mentioned before and the second may correspond to our 21.6-MeV peak.

The dominant peaks near 22.0, 23.8, and 25.5 MeV in Fig. 4 and also 22.7 and 25.5 MeV in Fig. 5 are considered to make up the giant dipole resonance. However, the single-particle-hole model has predicted only two electric dipole states at 23.09 and 24.89 MeV (Donnelly) in this energy region. The level at 23.09 MeV has a dominant ($1d_{5/2}$, $1p_{3/2}{}^{-1}$) configuration and corresponds in the collective model to the isospin oscillation which can be strongly excited by the longitudinal interaction. The other level at 24.89 MeV which has a dominant ($1d_{3/2}$, $1p_{3/2}{}^{-1}$) configuration corresponds to the spin-isospin oscillation, which is mainly excited by the transverse interaction.

The dipole strength of the isospin state may be redistributed among the 22.0-, 23.8-, and 25.5-MeV states observed. In order to obtain the form factor for these states, their resonance shape and the continuum background were estimated as shown in Fig. 6 (dashed curves). The sum of the longitudinal form factors for the 22.0- and 23.8-MeV excitations are compared with the theoretical form factor (Donnelly and KIA) in Fig. 15. The longitudinal form factor at the photon point obtained from the (γ, total) cross section[20] is also shown. Although these peaks are considered as almost pure 1^- states, the q dependence of their form factor observed shows a slight discrepancy from that of the theoretical 1^- form factor, particularly in the high-q region. A tendency for the calculated form factors to decrease too rapidly with increasing momentum transfer has already been pointed out by Donnelly.[28] According to his

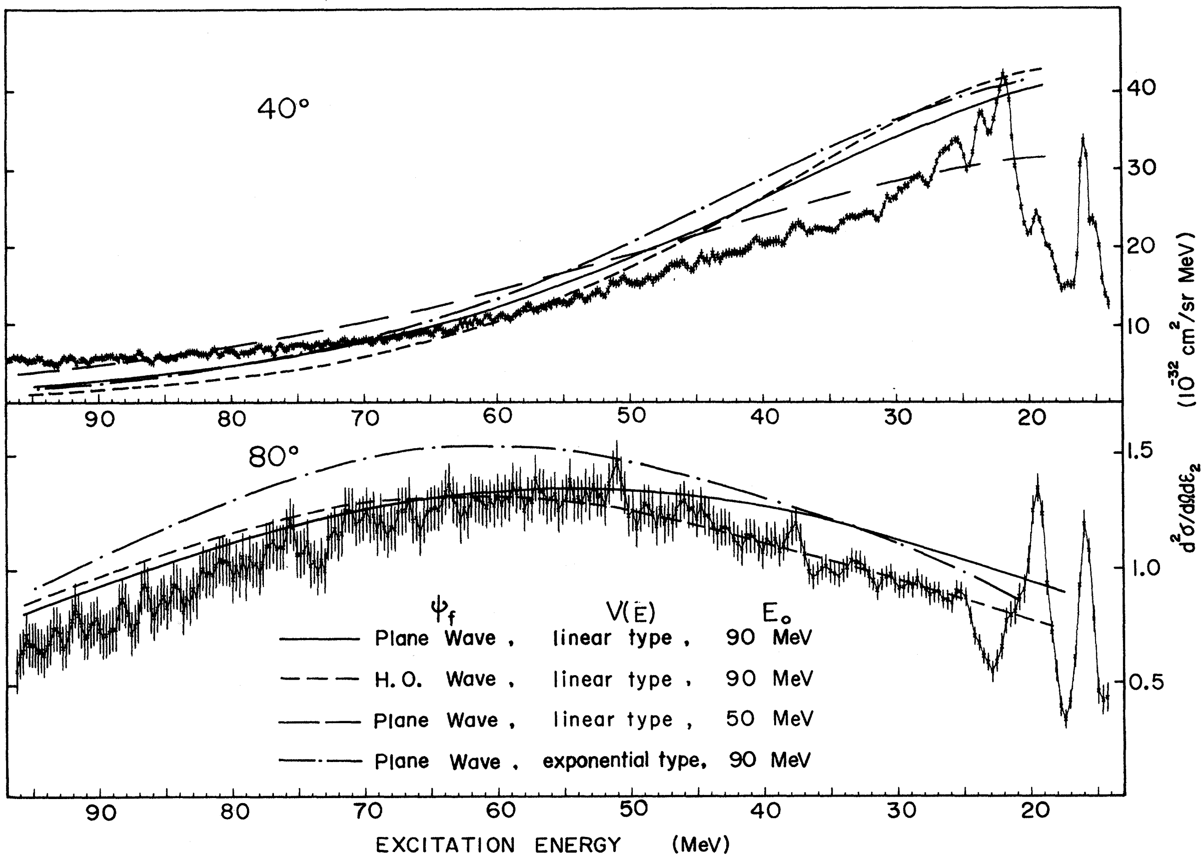

FIG. 21. Spectra of the scattered electrons at 40° (top) and 80° (bottom) from ^{12}C for an incident energy of 250 MeV. The spectra are compared with the predictions of the quasielastic model presented by de Forest. The curves correspond to the various combinations of the final-state wave functions and the energy-dependent potentials as listed in the lower part.

suggestion, it may be changed to some extent by the use of finite-well wave functions instead of the harmonic-oscillator wave functions.

The spin-isospin states may also redistribute among peaks, one of which seems to be the 22.7-MeV state. The 22.7-MeV form factor is compared with the theoretical σ-τ-state form factor (Donnelly and KIA) as shown in Fig. 16. As may be seen, the q dependence of the KIA form factor for this state is slightly different from the simple particle-hole-model case. Actually the 22.7-MeV form factor rather resembles the KIA 1^- σ-τ form factor. The other spin-isospin states may be distributed around 25.5 MeV as suggested by previous studies.[26, 33, 34] However, this peak becomes distinct as q is increased. It may correspond to the excitation of the predicted 25.09-MeV (3^-, $T=1$) state mentioned before. The 25-MeV complex seems to consist of the 1^- τ, 1^- σ-τ, and 3^- states.

The spins and parities identified by the present and previous studies are shown in the upper part of Figs. 4 and 5 where arrows indicate the position of the peaks. The excitation energies for the various multipole states calculated by the one-particle–one-hole calculation may be identified with the peaks excited by electron scattering except for the highest-lying state, for which the resonance width seems to be broad. The theoretical and observed energy levels (MeV) for $J^\pi=1^-$, 2^-, 3^-, and 4^-, $T=1$ in ^{12}C are listed in Table I. The even-parity states found by the present experiment are also compared with those predicted by the intermediate-coupling model in Table II. Also shown are the energies for the 1^+ and 2^+ states calculated by Gillet and Vinh Mau.[25]

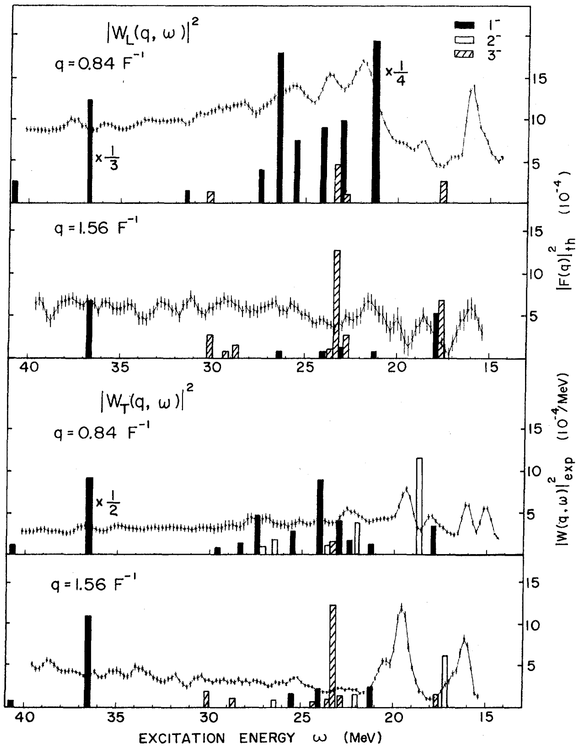

FIG. 22. The longitudinal and transverse form factors as functions of the excitation energy corresponding to $q=0.84$ and 1.56 F^{-1}. The position and strength for the KIA-model 1^-, 2^-, and 3^- states are shown.

The experimental longitudinal and transverse form factors in the energy regions 21–26 and 21–37 MeV are compared with the sum of the dipole form factors for the 23.09- and 24.89-MeV levels and the sum of those of the 23.09-, 24.89-, and 35.55-MeV levels (Donnelly), respectively, as shown in Figs. 19 and 20.

V. DISCUSSION

As mentioned in the previous section the simple particle-hole model fails to describe the fine structure in the giant-resonance region. The KIA model includes the additional effect of a coupling

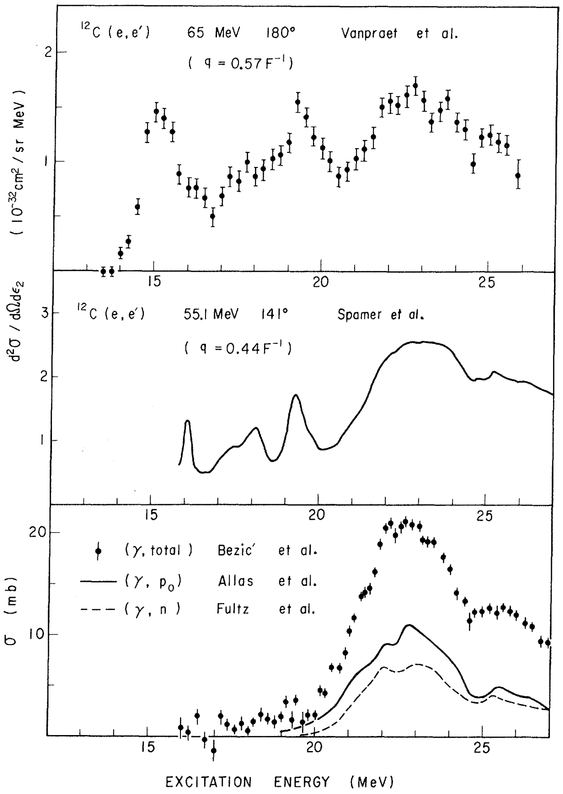

FIG. 23. The upper points show an inelastically scattered electron spectrum from ^{12}C at 180° (Ref. 9). The middle curve shows a (e,e') spectrum at 141° (Ref. 54). The lower curves show the cross sections for photoabsorption (Ref. 20); (γ,p_0) (Ref. 21); and (γ,n) (Ref. 19).

of the dipole excitations based on the ^{12}C ground state with those based on the lowest vibrational 4.43-MeV (2^+) state. The one-particle–one-hole states split to various states by the effect of this coupling as may be seen in Fig. 22.

Our longitudinal and transverse form factors at $q=0.84$ and 1.56 F^{-1} are compared with the schematic magnitude of the KIA form factor as shown in Fig. 22. As can be seen in the upper spectrum, the dipole isospin state seems to be split into three main peaks (22.0, 23.8, and 25.5 MeV) with almost the same strength, while the strength of KIA τ state concentrates too much on the one predicted at 21.2 MeV. The KIA model predicts many 3^- states, as shown in the spectra, where the momentum transfer is favorable for $E3$ excitation. The predicted 3^- states at 17.7 and 23.0 MeV with dominant $(d_{5/2}, p_{3/2}^{-1})$ and $(d_{3/2}, p_{3/2}^{-1})$ configurations, respectively, may correspond to the actual peaks at 18.6 and 25.5 MeV.

The possibility of the dipole spin-isospin mode was examined by many authors.[13, 26, 33, 34] The peak around 25.5 MeV has been considered as a candidate for this mode of excitation. In our transverse form factor, there may be seen resonances in the vicinity of 22.7 and 25.5 MeV. The q dependence of the 22.7-MeV form factor is quite similar to the feature of the 1^- σ-τ state predicted by the KIA model as mentioned before. The KIA model predicts sizable strength for the excitation of this state even at the photon point. As can be seen in Figs. 4 and 5, the position of the 22.7-MeV (σ-τ) state corresponds to the dip of the isospin excitation. Thus, the presence of this σ-τ state may be seen in the photoabsorption spectrum or in the low-q spectrum at large angles as a smooth peak near 22.7 MeV.

Figure 23 shows examples of such spectra obtained at Stanford[9] and Darmstadt[54] and reported by Bezić *et al.*[20] The Stanford data were taken at $\epsilon_1 = 65$ MeV and $\theta \approx 180°$. At $\theta \approx 180°$, only the transverse term contributes to the cross section, since the Mott cross section vanishes. Thus, this spectrum should be compared with our transverse form factor. Although there is a difference in the q values, agreement between the Stanford spectrum and ours is quite satisfactory. Our transverse form-factor peak at 22.7 MeV may be confirmed by this comparison.

The Darmstadt spectrum was obtained at $\epsilon_1 = 55.1$ MeV and $\theta = 141°$ where the transverse excitation is highly enhanced. Thus, this spectrum shows a complex of 22.0-MeV τ and 23.8-MeV τ and 22.7-MeV σ-τ states to be a broad resonance as seen in Fig. 23. Almost the same structure may also be seen in the (γ, total), (γ, p_0), and (γ, n) cross sections.

As mentioned above, the KIA model is superior to the simple particle-hole model. However, it may be unrealistic to consider the ground state for ^{12}C to be spherical. The (^{12}C, ^{12}C),[55] (p,p'),[56] and (e,e')[57] reactions show strong evidences for the possibility of the rotational band based on the ground state in ^{12}C. Nilsson, Sawicki, and Glendenning[58] have made calculations on the giant dipole transition by assuming ^{12}C to be an oblate spheroid. In strongly deformed nuclei, the dipole state splits into the separate groups corresponding to the characteristic frequencies along the major and minor axes of the nuclear spheroid.[59, 60] A great variety of states, with considerable dipole strength have been presented by Nilsson *et al.* which may explain the fine structure in the giant resonance. Recently Suzuki[61] has found that the dipole σ-τ state also splits into separate ones as in the case of the τ state in the deformed ^{12}C nucleus.

As can be seen from examples, such as for the 15.1-MeV (1^+), 16.1-MeV (2^+), 20.0-MeV (2^+), and 20.6-MeV (3^+) states, the intermediate-coupling model reproduces excellently the absolute magnitude of the experimental form factors. An attempt to describe the ^{12}C giant dipole resonance using the intermediate-coupling wave function has been made by Goncharova and Yudin[62] and by Rowe and Wong.[63, 64] These calculations show that the dipole strength distributes among a number of states which may reproduce the fine structure of the giant resonance. Such a splitting of the dipole states appears simply as a consequence of the intermediate-coupling shell-model character of the ground state. As mentioned before, the KIA and Nilsson states are due to a collective mechanism, such as dipole-quadrupole vibrational coupling or an intrinsic deformation of the ^{12}C ground state. The quite different approaches for the ^{12}C giant resonance display almost the same structure. However, all of the approximations show the trend for the dipole strength to be concentrated too much on the one or two close-lying dipole states, compared with experimental observation.

TABLE II. The observed and theoretical energy levels (MeV) for $J^\pi = 1^+$, 2^+, and 3^+, $T=1$ in ^{12}C.

J^π	Present work	Boyarkina (Ref. 29)	Gillet and Vinh Mau (Ref. 25)
1^+	15.1	15.5	16.6
		21.2	
2^+	16.1	16.6	16.3
		23.7	
	20.0	23.9	
		28.5	
3^+	20.6	21.0	
		24.5	

ACKNOWLEDGMENTS

The authors would like to express their thanks to Professor M. Kimura, director of this laboratory, for his continuous encouragement during the present work and also Professor S. Fujii for his valuable discussions and advice. They are also indebted to Professor J. Fujita for his valuable suggestions. They also thank T. Suzuki for his many helpful discussions and suggestions. Thanks are also due our friends in our laboratory for their helpful discussions. They are grateful to Professor Y. Kojima and his crew for the beam operation during the extended periods of measurement.

---

[1] W. C. Barber, Ann. Rev. Nucl. Sci. 12, 1 (1962).

[2] T. de Forest and J. D. Walecka, Advan. Phys. 15, 1 (1966).

[3] G. A. Proca and D. B. Isabelle, Nucl. Phys. A109, 177 (1968).

[4] G. R. Bishop and A. Bottino, Phys. Letters 10, 308 (1964).

[5] B. Dudelzak and R. E. Taylor, J. Phys. Radium 22, 544 (1961).

[6] W. C. Barber, F. Berthold, G. Fricke, and F. E. Gudden, Phys. Rev. 120, 2081 (1961).

[7] F. Gudden, Phys. Letters 10, 313 (1964).

[8] G. R. Bishop, Phys. Rev. Letters 19, 659 (1967).

[9] T. de Forest, J. D. Walecka, G. Vanpraet, and W. C. Barber, Phys. Letters 16, 311 (1965).

[10] G. A. Beer, T. E. Drake, R. M. Hutcheon, V. W. Stobie, and H. S. Caplan, Nuovo Cimento 53B, 7 (1968).

[11] J. Goldemberg and W. C. Barber, Phys. Rev. 134, B963 (1964).

[12] H. Crannell, H. A. Dahl, and F. H. Lewis, Jr., Phys. Rev. 155, 1062 (1967).

[13] G. Ricco, H. S. Caplan, R. M. Hutcheon, and R. Malvano, Nucl. Phys. A114, 685 (1968).

[14] J. Goldemberg, W. C. Barber, F. H. Lewis, Jr., and J. D. Walecka, Phys. Rev. 134, B1022 (1964).

[15] T. W. Donnelly, J. D. Walecka, I. Sick, and E. B. Hughes, Phys. Rev. Letters 21, 1196 (1968).

[16] Y. Torizuka, A. Yamaguchi, K. Nakahara, M. Oyamada, T. Terasawa, K. Itoh, Y. Kojima, and M. Kimura, Phys. Rev. 188, 1745 (1969).

[17] Y. Torizuka, A. Yamaguchi, T. Terasawa, Y. Kojima, K. Nakahara, M. Oyamada, K. Itoh, A. Nakada, S. Mitunobu, and M. Kimura, Phys. Rev. Letters 25, 874 (1970).

[18] B. C. Cook, J. E. E. Balgin, J. N. Bradford, and J. E. Griffin, Phys. Rev. 143, 724 (1966).

[19] S. C. Fultz, J. T. Caldwell, B. L. Berman, R. L. Bramblett, and R. R. Harvey, Phys. Rev. 143, 790 (1966).

[20] N. Bezić, D. Brajinik, D. Jamnik, and G. Kernel, Nucl. Phys. A128, 426 (1969).

[21] R. G. Allas, S. S. Hanna, L. Meyer-Schützmeister, and R. E. Segel, Nucl. Phys. 58, 122 (1964).

[22] G. Kernel and W. M. Mason, Nucl. Phys. A123, 205 (1969).

[23] T. de Forest, Nucl. Phys. A132, 305 (1969).

[24] N. Vinh Mau and G. E. Brown, Nucl. Phys. 29, 89 (1962).

[25] V. Gillet and N. Vinh Mau, Nucl. Phys. 54, 321 (1964).

[26] F. H. Lewis and J. D. Walecka, Phys. Rev. 133, B849 (1964).

[27] T. de Forest, Phys. Rev. 139, B1217 (1965).

[28] T. W. Donnelly, Phys. Rev. C 1, 833 (1970).

[29] A. N. Boyarkina, Izv. Akad. Nauk. SSSR Ser. Fiz. 28, 337 (1964) [transl.: Bull. Acad. Sci. USSR Phys. Ser. 28, 255 (1964)].

[30] M. Kamimura, K. Ikeda, and A. Arima, Nucl. Phys. A95, 129 (1967).

[31] H. Überall, Nuovo Cimento 41B, 25 (1966).

[32] H. Überall, Nuovo Cimento Suppl. 4, 781 (1966).

[33] J. L. Friar, Nucl. Phys. 84, 150 (1966).

[34] F. J. Kelly and H. Überall, Phys. Rev. 175, 1235 (1968).

[35] J. W. Lightbody, Jr., and S. Penner, Phys. Rev. Letters 24, 274 (1970).

[36] H. Ikegami, Rev. Sci. Instr. 29, 943 (1958).

[37] M. Sakai, Nucl. Instr. Methods 8, 61 (1960).

[38] H. Crannell, Phys. Rev. 148, 1107 (1966).

[39] J. Schwinger, Phys. Rev. 75, 898 (1949).

[40] H. Suura, Phys. Rev. 99, 1020 (1955).

[41] Y.-S. Tsai, Phys. Rev. 122, 1898 (1961).

[42] W. Heitler, *Quantum Theory of Radiation* (Clarendon Press, Oxford, England, 1960), 3rd ed.

[43] B. Rossi, *High-Energy Particles* (Prentice-Hall, Inc., Englewood Cliffs, New Jersey, 1965).

[44] D. B. Isabelle and G. R. Bishop, Nucl. Phys. 45, 209 (1963).

[45] R. Hofstadter, *Nuclear and Nucleon Structure* (W. A. Benjamin, Inc., New York, 1963).

[46] D. G. Ravenhall, quoted in R. Hofstadter, Rev. Mod. Phys. 28, 214 (1956).

[47] D. Kurath, Phys. Rev. 134, B1025 (1964).

[48] M. Hirooka, Ph.D. thesis, Osaka University, 1969 (unpublished).

[49] S. Cohen and D. Kurath, Nucl. Phys. 73, 1 (1965).

[50] M. Hirooka, T. Konishi, R. Morita, H. Narumi, M. Soga, and M. Morita, Progr. Theoret. Phys. (Kyoto) 40, 808 (1968).

[51] M. Chemtob and A. Lumbroso, Nucl. Phys. B17, 401 (1970).

[52] W. Feldman, M. Suffert, and S. S. Hanna, Bull. Am. Phys. Soc. 13, 882 (1968).

[53] J. Friar, quoted in Refs. 15 and 28.

[54] P. Antony-Spies, P. P. Delsanto, E. Spamer, A. Goldmann, and O. Titze, Phys. Letters 31B, 632 (1970).

[55] G. T. Garvery, A. M. Smith, and I. C. Hieber, Phys. Rev. 130, 2397 (1963).

[56] G. R. Satchler, Nucl. Phys. A100, 497 (1967).

[57] K. Nakahara *et al.*, Research Report, Laboratory of Nuclear Science, Tohoku University, 1969 (unpublished), Vol. 2, p. 1.

[58] S. G. Nilsson, J. Sawicki, and N. K. Glendenning, Nucl. Phys. 33, 239 (1961).

[59] K. Okamoto, Progr. Theoret. Phys. (Kyoto) 15, 75 (1956); Phys. Rev. 110, 143 (1958).

[60] M. Danos, Bull. Am. Phys. Soc. 1, 135 (1956); Nucl.

Phys. 5, 23 (1958).
[61] T. Suzuki, private communication.
[62] N. G. Goncharova and N. P. Yudin, Phys. Letters 29B, 272 (1969).
[63] D. J. Rowe and S. S. M. Wong, Phys. Letters 30B, 147 (1969).
[64] S. S. M. Wong and D. J. Rowe, Phys. Letters 30B, 150 (1969).

PHYSICAL REVIEW C VOLUME 3, NUMBER 5 MAY 1971

d-^{4}He Elastic Scattering at 12.000 MeV[*]

J. H. Jett, J. L. Detch, Jr.,[†] and Nelson Jarmie
Los Alamos Scientific Laboratory, University of California, Los Alamos, New Mexico 87544

(Received 4 January 1971)

Accurate cross-section measurements are presented for d-^{4}He elastic scattering at 12.000 MeV.

INTRODUCTION

As part of a continuing program of accurate cross-section measurements, we have measured d-α elastic scattering differential cross sections at 12.000 MeV. The average relative error for the data is 0.67% and the scale error is 0.52%. The data were taken at this energy to complement the tensor and vector analyzing power measurements of Lawrence *et al.*[1] The closest previous cross-section measurements were made by Senhouse and Tombrello[2] at 11.475 MeV with average relative errors of 2.7%.

METHOD

The deuteron beam from the Los Alamos tandem Van de Graaff accelerator passed through a gas target with thin Havar foil windows, and the scattered deuterons or α particles were detected by a single E-ΔE detector arrangement using solid-state detectors. Amplified pulses gated by the E-ΔE coincidence were digitized and sent to an on-line computer for mass analysis and storage. The resulting spectra were later analyzed for the yield.

The experimental apparatus used is described in detail by Jarmie *et al.*[3] and Detch.[4] The methods and techniques used for this experiment are as described in those references with the following exceptions. Due to the kinematics of the scattering, the energy of the deuterons at angles greater than 100° in the lab prevented detection of the deuterons with particle identification. Without particle identification, the background was too high and ill shaped to permit reasonable interpretation. Thus, in order to complete the angular distribution, we detected the α particles at lab angles from 12 to 35° (corresponding to deuteron center-of-mass angles from 156 to 110°). The agreement at the overlap angles is very good as is shown in Table I.

The detector efficiency was corrected for nuclear reactions based on the data of King *et al.*[5] This was done for both the detected deuteron and α particle. The largest correction was 0.3%.

TABLE I. Differential cross sections. $d+\alpha$ elastic scattering, 12.000 ± 0.015 MeV (20 keV FWHM).

θ_{lab} (deg)	$\sigma(\theta)_{\mathrm{lab}}$ (mb/sr)	$\theta_{\mathrm{c.m.}}$ (deg)	$\sigma(\theta)_{\mathrm{c.m.}}$ (mb/sr)	Relative error (%)	Absolute error (%)
12.00	984.5	18.03	441.8	0.72	0.90
15.00	702.1	22.51	318.0	0.34	0.62
20.00	397.4	29.95	183.7	0.42	0.67
25.00	194.9	37.33	92.51	0.47	0.70
30.00	76.14	44.63	37.33	0.62	0.81
35.00	22.57	51.84	11.50	1.06	1.16
40.00	12.74	58.94	6.786	1.04	1.16
45.00	24.23	65.92	13.58	0.74	0.91
50.00	43.50	72.75	25.82	0.73	0.90
55.00	62.09	79.42	39.28	0.62	0.81
60.00	74.69	85.92	50.68	0.59	0.78
65.00	79.19	92.21	57.97	0.58	0.77
70.00	75.18	98.30	59.74	0.61	0.80
75.00	66.35	104.16	57.55	0.61	0.80
80.00	53.90	109.78	51.28	0.62	0.80
35.00[a]	166.1	109.96	50.66	0.83	0.98
30.00[a]	126.5	119.96	36.50	0.64	0.82
90.00	31.25	120.28	36.21	0.67	0.85
100.00	18.75	129.77	26.73	0.76	0.92
25.00[a]	96.94	129.97	26.74	1.08	1.20
20.00[a]	107.0	139.97	28.43	0.57	0.77
17.50[a]	132.2	144.98	34.60	0.56	0.76
15.00[a]	167.9	149.98	43.39	0.57	0.76
12.00[a]	216.4	155.98	55.24	0.46	0.69

[a] At these angles, the recoil ^{4}He was detected. The center-of-mass angle listed is the corresponding deuteron angle.